

Lattice QCD calculation of the η and η' meson masses at the physical point using rooted staggered fermions

Willem E. A. Verplanke,¹ Zoltan Fodor,^{2,3,4,5} Antoine Gérardin,^{1,*} Jana N. Guenther,² Laurent Lellouch,¹ Kalman K. Szabo,³ Balint C. Toth,^{2,3} and Lukas Varnhorst²

¹*Aix-Marseille Université, Université de Toulon, CNRS, CPT, Marseille, France*

²*Department of Physics, University of Wuppertal, D-42119 Wuppertal, Germany*

³*Jülich Supercomputing Centre, Forschungszentrum Jülich, D-52428 Jülich, Germany*

⁴*Institute for Theoretical Physics, Eötvös University, H-1117 Budapest, Hungary*

⁵*Physics Department, Pennsylvania State University, University Park, PA 16802, USA*

We present a lattice calculation of the η and η' meson masses at the physical point and in the continuum limit, based on $N_f = 2 + 1 + 1$ flavors of rooted staggered quarks. Our analysis includes gauge ensembles at the physical pion and kaon masses spread over six lattice spacings in the range [0.064-0.1315] fm. Our main results read $m_\eta = 543.5(5.6)$ MeV and $m_{\eta'} = 986(38)$ MeV, consistent with the experimental values. This is an important numerical test that supports the validity of the fourth root procedure used in the staggered quark formalism. This calculation was the first step towards extracting the pseudoscalar transition form factors of the η and η' mesons that play a crucial role in the hadronic light-by-light contribution to the muon $g - 2$.

I. INTRODUCTION

In the chiral limit, where up, down and strange quark masses are set to zero, the classical Lagrangian of QCD exhibits an $SU(3)_L \times SU(3)_R \times U(1)_A \times U(1)_B$ global symmetry. In Nature, the $SU(3)_L \times SU(3)_R$ symmetry is spontaneously broken down to $SU(3)_V$, leading to eight Goldstone bosons, one for each broken generator. These Goldstone bosons can be identified with the octet of light pseudoscalar mesons ($\pi^0, \pi^\pm, K^0, \bar{K}^0, K^\pm, \eta$) and their different masses can be explained by the non-vanishing quark-mass matrix that explicitly breaks $SU(3)_f$ flavor symmetry. On the other hand, the $U(1)_A$ symmetry is anomalous [1, 2] and the flavor-singlet η' acquires a mass, even in the chiral limit. The origin of the singlet meson mass can be explained by the non-trivial topological structure of QCD and the existence of instantons [3, 4].

Flavor symmetry breaking also leads to mixing among the states with the same quantum numbers. The three neutral mesons π_3, η_0 and η_8 , defined in the chiral limit and with quantum numbers $J^{PC} = 0^{-+}$, mix to give the physical π^0, η and η' mesons observed experimentally. The mixing between the pion and the other two neutral mesons, proportional to $m_u - m_d$, is small and vanishes in the isospin limit. For the η and η' , $SU(3)_f$ breaking effects are more important and both mesons can be seen as a mixture of the η_0 and η_8 states. Only in the $SU(3)_f$ symmetric limit can one perform the assignment $\eta = \eta_8$ and $\eta' = \eta_0$. In addition, one would expect mixing with glueballs with quantum numbers $J^{PC} = 0^{-+}$. However, due to their large masses, above 2.5 GeV as suggested by lattice calculations [5, 6], this mixing is not considered in this study.

Reproducing the mass of the η and η' mesons from first-principle using lattice QCD simulations is an important test of our understanding of the chiral symmetry breaking mechanism and the complex topological structure of QCD [7]. However lattice calculations of the flavor-singlet meson masses are challenging due to the presence of large quark-disconnected contributions and large autocorrelation times, especially for the η' meson. The spectrum has been studied for a long time on the lattice using $N_f = 2 + 1$ domain-wall fermions [8, 9], $N_f = 2 + 1 + 1$ twisted-mass fermions [10–12] and $N_f = 2 + 1$ Wilson-clover quarks [13–15]. However, the spectrum has never been computed directly at the physical pion mass and the results quoted at the physical point rely on a chiral extrapolation. There is also less literature for rooted staggered quarks despite its relevance in assessing the validity of the rooting procedure and the ability of staggered quarks to reproduce the $U(1)_A$ anomaly correctly. A first attempt was presented in [16] using two gauge

* antoine.gerardin@cpt.univ-mrs.fr

ensembles with different pion masses and lattice spacings. The result suggests a good agreement with experiment but lacks a proper extrapolation to the physical point. In [17], the validity of rooting has been investigated through the massive Schwinger model with a single flavor where the corresponding η meson acquires a mass through the axial anomaly. Finally, in [18], the authors analyzed the behavior of flavor-singlet and taste-singlet correlators by looking at the near-zero modes of the Dirac operator.

Staggered transformations [19] can be used to diagonalize, in spinor space, the naive discretization of the Dirac operator in any background gauge field (see [20, 21] for a review). For each flavor, the resulting single-component spinor field reduces the number of doublers from 16 to 4, called tastes, and allows for much faster numerical implementations at the cost of having extra tastes that need to be eliminated. In the continuum limit, all tastes are expected to be equivalent and we are left with an exact fourfold degeneracy of quarks per staggered fermion field. In practice, to further reduce the number of tastes from four to one in the sea, one usually takes the fourth root of the fermion determinant, for each flavor introduced in the simulation. This method, called *rooting*, is justified in the continuum limit due to the exact fourfold degeneracy [22] such that the determinant of each flavor factorizes into four identical determinants representing a single fermion. However, this step is more controversial at finite lattice spacings where taste violation effects break the degeneracy among tastes, leading to a non-unitary theory [23, 24]. These unphysical effects are, however, expected to vanish in the continuum limit [22, 25–28]. Since most arguments against rooting involve the axial anomaly, the η' meson plays a central role.

This work is also a first step toward the lattice calculation of the pseudoscalar transition form factors [29] that are key inputs to evaluate the hadronic light-by-light scattering contribution in the muon $g - 2$ [30, 31].

The rest of this paper is organized as follows. In Section II, we present the methodology to extract the η and η' meson masses from lattice QCD simulations. In Section III we discuss the implementation of two staggered taste-singlet pseudoscalar interpolating operators and we present the different noise-reduction techniques that have been implemented to evaluate the noisy quark-disconnected contributions. In Section IV, we start with a comparison of the two taste-singlet operators, focusing on the quark-connected contribution. In Section V, we present our results for the spectrum on individual gauge ensembles, where different strategies to extract the masses are discussed. Finally, we extrapolate the data to the continuum limit before concluding in Section VI.

II. METHODOLOGY

We work in the isospin limit of QCD defined by $m_l \equiv m_u = m_d$ and electromagnetic interactions are neglected such that the pion does not mix with the η and η' pseudoscalars. In this limit, the η meson is a stable particle as the hadronic decays $\eta \rightarrow \pi^+\pi^-\pi^0$ and $\eta \rightarrow 3\pi^0$ break isospin symmetry. However, because the η' is significantly heavier than the η , the strong decays $\eta' \rightarrow \eta\pi^+\pi^-$ and $\eta' \rightarrow \eta\pi^0\pi^0$ are allowed. In this paper, we nevertheless treat the η' meson as a stable particle. This approximation is well justified since the decay width 0.188(6) MeV [32] is small compared to the resolution we are aiming for in this work. The charm quark contribution was shown to be small by the ETM collaboration [10] and is thus neglected here.

There is a lot of freedom regarding the choice of interpolating operators, with the only requirement that they should have non-zero overlap with the physical states of interest. For the pion, we consider the flavor structure

$$P_3(x) = \frac{1}{\sqrt{2}} (\bar{u}\gamma_5 u(x) - \bar{d}\gamma_5 d(x)) = \bar{\psi}(x) \frac{\lambda_3}{2} \psi(x), \quad (1)$$

where $\bar{\psi} = (\bar{u}, \bar{d}, \bar{s})$ is a vector in flavor space and λ_a are the Gell-Mann matrices. For the $\eta^{(\prime)}$, a standard choice of interpolating operators is given by the flavor-octet η_8 and flavor-singlet η_0

operators

$$P_8(x) = \frac{1}{\sqrt{6}} (\bar{u}\gamma_5 u(x) + \bar{d}\gamma_5 d(x) - 2\bar{s}\gamma_5 s(x)) = \bar{\psi}(x) \frac{\lambda_8}{2} \psi(x), \quad (2a)$$

$$P_0(x) = \frac{1}{\sqrt{3}} (\bar{u}\gamma_5 u(x) + \bar{d}\gamma_5 d(x) + \bar{s}\gamma_5 s(x)) = \bar{\psi}(x) \frac{\lambda_0}{2} \psi(x), \quad (2b)$$

where $\lambda_0 = \frac{2}{\sqrt{3}}\mathbf{I}$. In the SU(3) flavor limit, $\langle 0|P_8|\eta_0\rangle = \langle 0|P_0|\eta_8\rangle = 0$, and the time dependence of the two-point correlation functions built from these operators is governed by the η_8 and η_0 mesons at large Euclidean times. The lattice implementation of those operators, projected on given spatial momenta, are denoted by O_3 , O_8 and O_0 and their specific forms will be discussed in Section III C. Away from the SU(3) flavor limit, the flavor-singlet and flavor-octet states mix to give the physical η and η' mesons, and we are left with the following correlation matrix

$$C_I(t) = \begin{pmatrix} \langle O_8(t)O_8^\dagger(0)\rangle & \langle O_8(x)O_0^\dagger(0)\rangle \\ \langle O_0(t)O_8^\dagger(0)\rangle & \langle O_0(x)O_0^\dagger(0)\rangle \end{pmatrix}. \quad (3)$$

In this isospin basis, the correlators are given by

$$\langle O_8(t)O_8^\dagger(0)\rangle = \frac{1}{3} (\mathcal{C}_l + 2\mathcal{C}_s + 2\mathcal{D}_{ll} + 2\mathcal{D}_{ss} - 2\mathcal{D}_{ls} - 2\mathcal{D}_{sl}) \quad (4a)$$

$$\langle O_8(t)O_0^\dagger(0)\rangle = \frac{\sqrt{2}}{3} (\mathcal{C}_l - \mathcal{C}_s + 2\mathcal{D}_{ll} - \mathcal{D}_{ss} + \mathcal{D}_{ls} - 2\mathcal{D}_{sl}) \quad (4b)$$

$$\langle O_0(t)O_8^\dagger(0)\rangle = \frac{\sqrt{2}}{3} (\mathcal{C}_l - \mathcal{C}_s + 2\mathcal{D}_{ll} - \mathcal{D}_{ss} + \mathcal{D}_{sl} - 2\mathcal{D}_{ls}) \quad (4c)$$

$$\langle O_0(x)O_0^\dagger(0)\rangle = \frac{1}{3} (2\mathcal{C}_l + \mathcal{C}_s + 4\mathcal{D}_{ll} + \mathcal{D}_{ss} + 2\mathcal{D}_{ls} + 2\mathcal{D}_{sl}) \quad (4d)$$

where \mathcal{C}_f is the quark-connected contribution of flavor f and $\mathcal{D}_{f_1 f_2}$ is the disconnected contribution with flavors f_1 and f_2 in each quark loop (see Fig. 2). The observation that this matrix is off-diagonal away from the SU(3)_f symmetric point underlines the fact that the SU(3) octet and singlet states are not eigenstates but mix to give the physical η and η' mesons. Neglecting for a moment higher excited states, that are exponentially suppressed at large Euclidean time, and oscillating contributions from the opposite parity channel that are specific to staggered quarks, the masses can be extracted from the time dependence of the correlation matrix

$$\langle O_a(t)O_b^\dagger(0)\rangle = \frac{Z_\eta^{(a)} Z_\eta^{(b)*}}{2E_\eta} e^{-E_\eta t} + \frac{Z_{\eta'}^{(a)} Z_{\eta'}^{(b)*}}{2E_{\eta'}} e^{-E_{\eta'} t} + \dots \quad (5)$$

where the four overlap factors are defined by $Z_n^{(i)} = \langle n|O_i|0\rangle$. On the lattice, it is often more natural to work in the flavor basis

$$P_l(x) = \frac{1}{\sqrt{2}} (\bar{u}\gamma_5 u(x) + \bar{d}\gamma_5 d(x)), \quad P_s(x) = \bar{s}\gamma_5 s(x), \quad (6)$$

where the correlation matrix, in terms of the corresponding lattice interpolating operators O_l and O_s , takes the simpler form

$$C_F(t) = \begin{pmatrix} \langle O_l(t)O_l^\dagger(0)\rangle & \langle O_l(x)O_s^\dagger(0)\rangle \\ \langle O_s(t)O_l^\dagger(0)\rangle & \langle O_s(x)O_s^\dagger(0)\rangle \end{pmatrix} = \begin{pmatrix} \mathcal{C}_{ll} + 2\mathcal{D}_{ll} & \sqrt{2}\mathcal{D}_{ls} \\ \sqrt{2}\mathcal{D}_{sl} & \mathcal{C}_{ss} + \mathcal{D}_{ss} \end{pmatrix}. \quad (7)$$

Since we are eventually interested in the extraction of the pseudoscalar transition form factors, the mixing between the two mesons is defined in terms of amplitudes for the pseudoscalar densities. In the flavor basis, this mixing can be described in terms of two constants and two angles

$$\begin{pmatrix} Z_\eta^{(l)} & Z_\eta^{(s)} \\ Z_{\eta'}^{(l)} & Z_{\eta'}^{(s)} \end{pmatrix} = \begin{pmatrix} c_l \cos \phi_l & -c_s \sin \phi_s \\ c_l \sin \phi_l & c_s \cos \phi_s \end{pmatrix}, \quad (8)$$

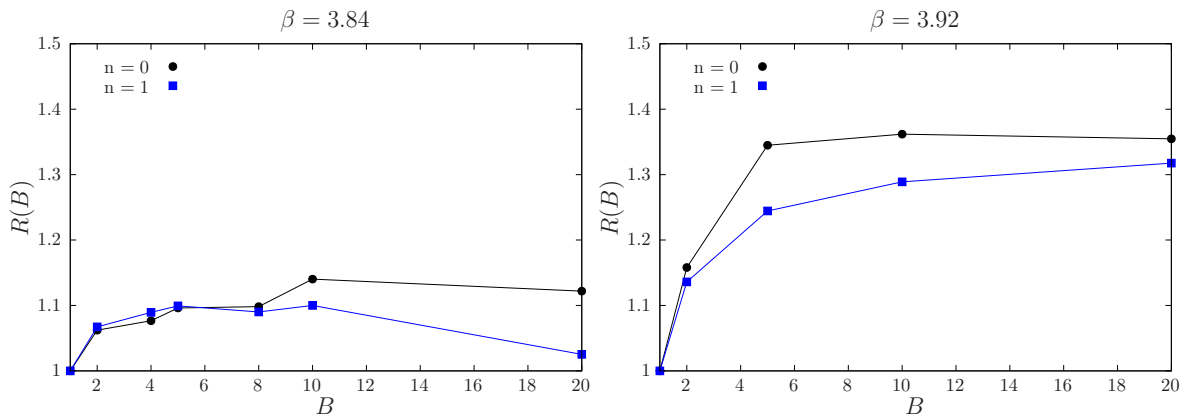


Figure 1. Normalized jackknife error as a function of bin size for the quantity $R(B) = \sum_{t=t_1}^{t_2} \mathcal{D}_{ll}(t/a)$ and for momenta $|\vec{p}| = n(2\pi/L)$, $n = 0, 1$. We use $t_1 = 2a$ and $t_2 = 8a$. The bin sizes used in the final analysis for these ensembles (in units of configurations separated by 10 trajectories) are 20 and 10 respectively.

with $\tan \phi_l = Z_{\eta'}^{(l)} / Z_{\eta}^{(l)}$, $\tan \phi_s = -Z_{\eta}^{(s)} / Z_{\eta'}^{(s)}$. Due to correlation among data, one expects to have a smaller statistical error on the geometric mean, $\tan^2 \phi_F = -(Z_l^{(\eta')} Z_s^{(\eta)})(Z_l^{(\eta)} Z_s^{(\eta')})$, rather than on ϕ_l and ϕ_s separately [11, 33].

Finally, in finite volume, the correlation functions can acquire a t -independent fully-disconnected contribution due to a partial sampling of the topological charge [14, 34]. Thus, in addition to the correlation matrix itself, we also consider the subtracted correlator $\overline{C}_{ij}(t) = C_{ij}(t + \Delta t) - C_{ij}(t)$ with $\Delta t/a = 1, 2$ [12, 15]. This subtraction also tends to reduce correlations between consecutive time slices, leading to more stable fits in Section V.

III. LATTICE SETUP

A. Lattice gauge ensembles

Our calculation is based on a subset of ensembles generated by the Budapest-Marseille-Wuppertal collaboration [35]. They have been generated using $N_f = 2 + 1 + 1$ dynamical staggered fermions with four steps of stout smearing. The bare quark masses have been tuned such that the Goldstone mesons are at nearly physical pion and kaon mass. The lattice spacing is set using the Ω baryon mass and we exploit six values of the lattice spacing in the range $[0.0640 - 0.1315]$ fm to extrapolate our result to the continuum limit. We consider large volumes with $L > 6$ fm where finite-volume effects will be shown to be negligible. Simulations are performed in the isospin limit where $m_u = m_d \equiv m_l$. More details about these ensembles can be found in [35, 36] and the main properties relevant for this work are summarized in Table I.

Statistical errors are estimated using the jackknife method after blocking the data over consecutive gauge field configurations. In Fig. 1 we present the statistical error of the light-quark disconnected correlator \mathcal{D}_{ll} as a function of the bin size. The block size is large enough to essentially suppress all visible autocorrelations. At our finest lattice spacing, the relatively small number of configurations might however hide longer range autocorrelations, especially for the η' meson.

B. Conventions

In this section we summarize the main definitions to set the notations used in this paper. For a review on staggered quarks, we refer the reader to [20, 22]. The staggered Dirac operator for a quark of flavor f , that acts on a single component spinor field χ with a background gauge

Table I. Parameters of the simulations: the bare coupling $\beta = 6/g_0^2$, the lattice resolution, the lattice spacing a and the spatial extent L in physical units, the bare light and strange quark masses and the number of gauge configurations. Only the large-volume ensembles with $L > 6$ fm are included in the final analysis. Ensembles with smaller physical extents are given for completeness and were used in [29].

β	$(L/a)^3 \times (T/a)$	a [fm]	L [fm]	am_l	am_s	#confs
3.7000	$48^3 \times 64$	0.1315	6.3	0.00205349	0.0572911	900
	$32^3 \times 64$		4.2	0.00205349	0.0572911	900
	$24^3 \times 48$		3.2	0.00205349	0.0572911	700
3.7500	$56^3 \times 96$	0.1191	6.7	0.00184096	0.0495930	500
	$56^3 \times 96$		6.7	0.00176877	0.0516173	500
	$56^3 \times 96$		6.7	0.00184096	0.0516173	500
3.7553	$56^3 \times 84$	0.1116	6.2	0.00171008	0.0476146	500
	$56^3 \times 84$		6.2	0.00171008	0.0485669	500
	$56^3 \times 84$		6.2	0.00174428	0.0461862	500
	$28^3 \times 56$		3.1	0.00171008	0.0476146	850
3.8400	$64^3 \times 96$	0.0952	6.1	0.00151556	0.0431935	500
	$64^3 \times 96$		6.1	0.001455	0.04075	1100
	$32^3 \times 64$		3.0	0.00151556	0.0431935	1100
	$32^3 \times 64$		3.0	0.00143	0.0431935	1050
	$32^3 \times 64$		3.0	0.001455	0.04075	1100
	$32^3 \times 64$		3.0	0.001455	0.03913	1100
3.9200	$80^3 \times 128$	0.0787	6.3	0.001172	0.03244	500
	$80^3 \times 128$		6.3	0.0012	0.0332856	500
	$40^3 \times 80$		3.1	0.001207	0.032	550
	$40^3 \times 80$		3.1	0.0012	0.0332856	350
4.0126	$96^3 \times 144$	0.0640	6.1	0.000977	0.0264999	500
	$96^3 \times 144$		6.1	0.001002	0.027318	450
	$48^3 \times 96$		3.1	0.00095897	0.0264999	850
	$48^3 \times 96$		3.1	0.001002	0.027318	450

field $U_\mu(x)$ reads

$$D_f(x, y) = \frac{1}{2a} \sum_{\mu} \eta_{\mu}(x) \left[U_{\mu}(x) \delta_{x+a\hat{\mu}, y} - U_{\mu}^{\dagger}(x - a\hat{\mu}) \delta_{x-a\hat{\mu}, y} \right] + m_f \delta_{x, y}, \quad (9)$$

where a is the lattice spacing, m_f the bare quark mass and $\eta_{\mu}(x)$ are phase factors satisfying $\Omega^{\dagger}(x) \gamma_{\mu} \Omega(x) = \eta_{\mu}(x)$ with $\Omega(x) = \gamma_1^{x_1/a} \gamma_2^{x_2/a} \gamma_3^{x_3/a} \gamma_4^{x_4/a}$ and γ_{μ} are the usual gamma matrices. In Eq. (9), the index μ runs from 1 to 4 and $\hat{\mu}$ denotes the unit vector in the direction μ . The fermionic action for the flavor f can be written in term of the Dirac operator as

$$\mathcal{S}_f = a^4 \sum_{x, y} \bar{\chi}(x) D_f \chi(y). \quad (10)$$

In the following, we use the conventions where

$$\eta_1(x) = 1, \quad \eta_2(x) = (-1)^{x_1/a}, \quad \eta_3(x) = (-1)^{(x_1+x_2)/a}, \quad \eta_4(x) = (-1)^{(x_1+x_2+x_3)/a}. \quad (11)$$

It is useful to note that $D^{\dagger}(y, x) = \epsilon(x) D(x, y) \epsilon(y)$ where $\epsilon = (-1)^{(x_1+x_2+x_3+x_4)/a}$ is the parity factor. This property is similar the γ_5 -hermiticity of the Wilson Dirac propagator and it holds on a single gauge configuration.

C. Pseudoscalar interpolating operators

The pseudoscalar two-point correlation function involves Wick contractions with quark-disconnected contributions where quark and anti-quarks annihilates into gluons, see Fig. 2.

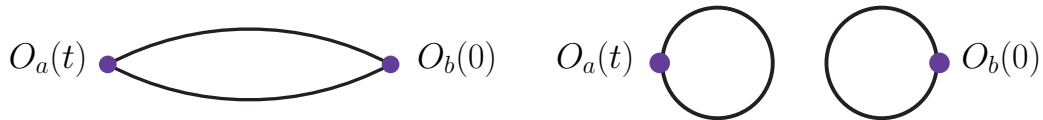


Figure 2. Connected and quark-disconnected contributions to the pseudoscalar two-point correlation functions in Eq. (3).

As low-energy gluons are taste singlets, such contributions require the use of taste-singlet pseudoscalar operators [18]. Using the notations of [20], where operators are given in the spin-taste basis as $\Gamma_S \otimes \Gamma_T$, two appropriate choices are given by the 3-link $\gamma_4 \gamma_5 \otimes 1$ and the 4-link $\gamma_5 \otimes 1$ operators [37]. The 3-link interpolating operator \hat{O}_3 is explicitly given by

$$O_3(x) = \frac{1}{6} \sum_{i,j,k} \epsilon_{ijk} \bar{\chi}(x) [\eta_i \Delta_i [\eta_j \Delta_j [\eta_k \Delta_k]]] \chi(x) \equiv \bar{\chi}(x) \hat{O}_3 \chi(x) \quad (12)$$

where $\Delta_\mu \chi(x) = \frac{1}{2} [U_\mu(x) \chi(x + a\hat{\mu}) + U_\mu^\dagger(x - a\hat{\mu}) \chi(x - a\hat{\mu})]$ is the symmetric shift operator and ϵ_{ijk} is the rank-3 Levi-Civita tensor. In order to maintain Lorentz covariance, we average over all equivalent shortest paths in Eq. (12) with a factor given by the sign of the permutation (i, j, k) . Gauge invariance is ensured by the insertion of the gauge field in the symmetric shift. The 4-link operator \hat{O}_4 is non-local in time and reads

$$O_4(x) = \frac{1}{2} \eta_4(x) \left[\bar{\chi}(x) \hat{O}_3 \chi_+(x) + \bar{\chi}_+(x) \hat{O}_3 \chi(x) \right] \quad (13)$$

where $\chi_+(x) = U_4(x) \chi(x + a\hat{t})$ and $\bar{\chi}_+(x) = \bar{\chi}(x + a\hat{t}) U_4^\dagger(x)$. The two-point correlation functions are built using either the 3-link or the 4-link pseudoscalar operator both at the source and at the sink. We have not considered the case where different operators are used at the source and at the sink. A comparison of the results given by the two operators is provided in Section IV A.

D. Staggered correlation functions

The light and strange quark-connected contributions are evaluated using $U(1)$ stochastic sources with support on a single time slice (time dilution) and the correlators are explicitly symmetrized in time with respect to $T/2$. For the quark-disconnected contributions, several gauge noise reduction techniques have been investigated. We have implemented low-mode averaging (LMA) [38, 39] where the quark propagator is written as $S_f = S_f^{(\text{lm})} + S_f^{(\text{hm})}$ and

$$S_f^{(\text{lm})}(x, y) = \sum_{n=1}^{N_{\text{ev}}} \frac{\phi_n(x) \phi_n^\dagger(y)}{\lambda_n + m_f} \quad (14)$$

is the low-mode contribution, expressed in term of the N_{ev} lowest eigenvectors ϕ_k and corresponding eigenvalues λ_n of the massless Dirac operator. The normalization $\sum_x \phi_n^\dagger(x) \phi_m(x) = \delta_{n,m}$ is used. This expression provides an exact estimator of the all-to-all propagator in the space spanned by the N_{ev} eigenvectors and volume averaging significantly reduces the statistical uncertainty. In practice, we use 1000 eigenvectors of the even-odd Dirac operator on our $L = 6$ fm ensembles. For smaller volumes, the number of eigenmodes is roughly rescaled by the volume ratio. The high-mode contribution to the quark propagator can be estimated stochastically using a set of N_s random sources η_s

$$S_f^{(\text{hm})}(x, y) = \frac{1}{N_s} \sum_{s=1}^{N_s} (D^{-1} P \eta_s)(x) \eta_s^\dagger(y), \quad P = 1 - \sum_{n=1}^{N_{\text{ev}}} \phi_n \phi_n^\dagger, \quad (15)$$

with P the projector orthogonal to the space spanned by the N_{ev} eigenvectors. In practice the stochastic sources used to estimate the disconnected contribution have support on the whole

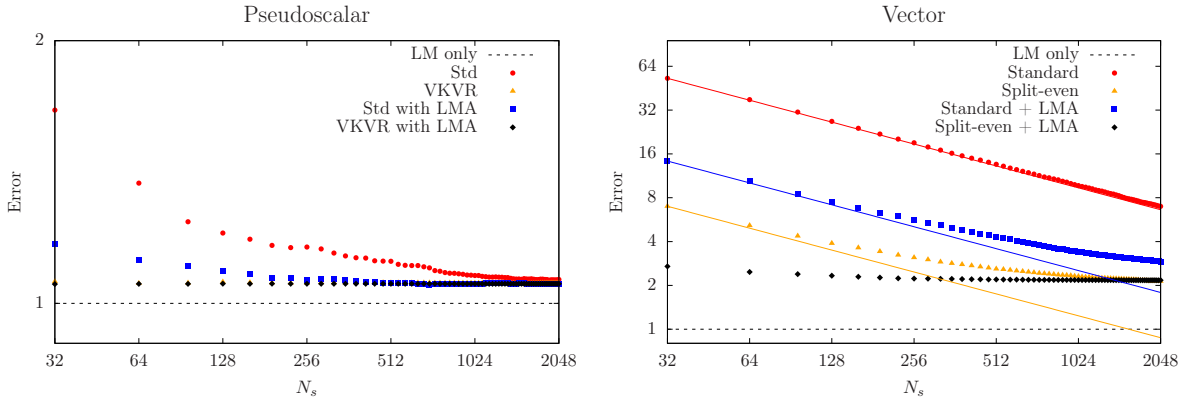


Figure 3. Comparison of the square root of the variance of the pseudoscalar (left) and vector (right) loops functions as a function of the number of stochastic sources N_s for the different estimators described in the text. For the vector loop, we present the results for the “light minus strange” flavor difference. The lines represent a perfect scaling of the variance assuming the variance is dominated by the stochastic noise. The horizontal dashed line is the error from the low-mode contribution only and is used as a normalization scale.

lattice and time dilution is not used there. To further reduce the numerical cost of the high-mode contribution to the quark loops, we have also implemented the all-mode averaging (AMA) technique [40–42]. For an observable \mathcal{O} , we use the decomposition (exact in the infinite statistics limit)

$$\langle \mathcal{O} \rangle = \langle \mathcal{O}_{\text{sloppy}} \rangle + \langle \mathcal{O}_{\text{cor}} \rangle, \quad (16)$$

where

$$\mathcal{O}_{\text{sloppy}} = \frac{1}{N_1} \sum_{s=1}^{N_1} \mathcal{O}_{\text{lp}}^{(s)}, \quad \mathcal{O}_{\text{cor}} = \frac{1}{N_2} \sum_{s=N_1+1}^{N_1+N_2} \left(\mathcal{O}_{\text{hp}}^{(s)} - \mathcal{O}_{\text{lp}}^{(s)} \right). \quad (17)$$

In general, the estimator \mathcal{O} requires the evaluation of quark propagators. For a given source (s), the estimator $\mathcal{O}_{\text{lp}}^{(s)}$ is then defined by a fix number of deflated conjugate gradient iterations while $\mathcal{O}_{\text{hp}}^{(s)}$ is obtained with exact (high precision) solves. In the correction term, the same stochastic noise is used for both low and high precision solves to maintain statistical correlations. The number of iterations defining the sloppy solves is tuned such that the correction term is small as compared to the statistical precision. In practice, we use 600 iterations at our finest lattice spacing while exact solves are defined by a residual smaller than 10^{-8} . It is thus numerically beneficial to use $N_1 \gg N_2$. It appears that AMA leads to a modest gain for pseudoscalar loops. However, it is very efficient for the vector loops that require many more inversions of the Dirac operator. Although those vector loops are not used in the work presented here, they are needed for the calculation of the light pseudoscalar transition form factors presented in [29].

Finally, when using the 4-link operator, we have implemented the Venkataraman-Kilcup variance reduction trick introduced in [43, 44] to estimate the stochastic part of the disconnected contribution. Noting that both the 4-link operator O_4 and $(D^\dagger D)^{-1}$ connects sites that are separated by an even number of gauge links, we obtain

$$\text{Tr} [O_4 D^{-1}] = \text{Tr} [O_4 (D^\dagger D)^{-1} D^\dagger] \approx m_f \frac{1}{N_s} \sum_s \psi_s^\dagger (O_4 \psi_s), \quad (18)$$

with $\psi_s = D^{-1} \eta_s$, the solution vector for the source (s). The last equality is valid only in the limit of infinite statistics and we note that the hopping term of the Dirac operator does not contribute such that the final estimator gets an explicit quark mass factor. An important feature of the VKVR trick is that it can be used for each flavor independently.

The various methods have been tested for both the pseudoscalar operator O_4 and for the conserved vector current

$$J_\mu(x) = -\frac{1}{2}\eta_\mu(x) \left[\bar{\chi}(x + a\hat{\mu})U_\mu^\dagger(x)\chi(x) + \bar{\chi}(x)U_\mu(x)\chi(x + a\hat{\mu}) \right]. \quad (19)$$

The comparison is performed at the level of the loop functions used to evaluate the disconnected diagrams. More precisely, we compute the quantities

$$L_4^{(f)}(t) = -\frac{1}{2} \left(\frac{a}{L} \right)^3 \sum_{\vec{x}} \eta_4(x) \text{Tr} \left[\hat{O}_3 U_4(x) S_f(x + a\hat{t}, x) + U_4^\dagger(x) \hat{O}_3 S_f(x, x + a\hat{t}) \right], \quad (20a)$$

$$L_{V;\mu}^{(f)}(t) = +\frac{1}{2} \left(\frac{a}{L} \right)^3 \sum_{\vec{x}} \eta_\mu(x) \text{Tr} \left[S_f(x, x + a\hat{\mu}) U_\mu^\dagger(x) + S_f(x + a\hat{\mu}, x) U_\mu(x) \right], \quad (20b)$$

where S_f is the quark propagator with flavor f . The results are shown in Fig. 3. For pseudoscalar loops, the VKVR trick is extremely efficient and performs better than LMA. With 32 sources, we already reach the gauge noise. For vector loops, the VKVR trick is not applicable and LMA leads to a significant gain. If one is only interested in the light minus strange flavor difference [29], as often happens with electromagnetic currents, then the split-even estimator introduced in [45] can be combined with LMA (see Appendix B of [29]). With this improved estimator, one can see in Fig. 3 that the gauge noise is reached for $N_s < 100$ stochastic sources.

IV. TASTE SINGLET PION AND TASTE SPLITTING

The staggered quark transformation reduces the number of tastes from 16 to 4 such that we are left with 16 pions that differ by tastes. In the continuum limit all tastes have equal mass but, at finite lattice spacing, taste interactions break this degeneracy. The Goldstone pion, with pseudoscalar taste ($\gamma_5 \otimes \gamma_5$) is the lightest pion and its mass has been tuned close to the physical pion mass in our simulations. Instead, the taste-singlet pion is the heaviest and its mass goes to the physical pion mass only in the continuum limit.

A. Comparison of the 3-link and 4-link operators

In this section we compare the 3-link and the 4-link operators, introduced in Section III C, for the taste-singlet pion where only the light quark-connected diagram contributes. In general, a staggered correlation function projected on a given spatial momenta presents oscillations in time due to the contribution of the parity partner state that appears with an extra factor $(-1)^{t/a}$. Neglecting excited states, the staggered correlator can be described by

$$C(t; \vec{p}) = A \cosh(E_1(\vec{p})[T/2 - t]) + (-1)^{t/a} B \cosh(E_2(\vec{p})[T/2 - t]), \quad (21)$$

where E_1 and E_2 are the energies of the pion and its parity partner state, T is the time extent of the lattice and A and B are some constant coefficients that depend on the details of the interpolating operator. Therefore, in the presence of an oscillating term, we define the smeared correlation function

$$\tilde{C}(t) = \frac{1}{4}C(t-a) + \frac{1}{2}C(t) + \frac{1}{4}C(t+a), \quad (22)$$

that projects (approximately) onto the pion state. With this definition, the suppression of the parity partner state is $O(a^2)$ and the effective mass can be defined by the usual logarithmic derivative of the smeared correlator.

In the left panel of Fig. 4, we compare the effective mass for both the 3- and 4-link operators. In [37] it was argued that the contribution of the parity partner state to the 4-link operator is strongly suppressed, a statement supported by our data where no oscillations are visible at all.

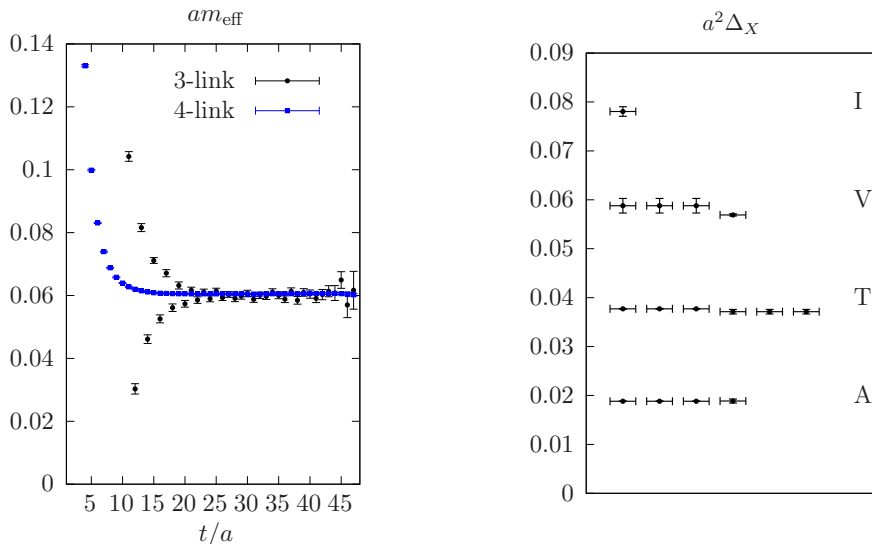


Figure 4. Left panel: effective mass plot for the 3-link and 4-link operators at our finest lattice spacing (note that a higher statistics is used for the 4-link operator). Right panel: mass splitting in the pion spectrum at our coarsest lattice spacing. The labels $X \in (P,A,T,V,I)$ refer to pseudoscalar, axial, tensor, vector and singlet tastes. The multiplet structure predicted by LO rS χ PT is clearly observed.

Thus, for the 4-link operator, the effective mass is obtained using the original correlator and the smearing in Eq. (22) is only applied to the 3-link operator. As expected, both operators lead to compatible values of the pseudoscalar mass. The 4-link operator presents two advantages: first the plateau is reached at earlier times and does not exhibit oscillations, second, the VKVR trick described above is applicable for the disconnected contribution. For these reasons, only the 4-link operator is used in our analysis of the $\eta^{(\prime)}$ mesons described below.

B. Pion mass and taste-breaking effects

At our coarsest lattice spacing, we have computed the full pion spectrum and the result is shown on the right panel of Fig. 4. We observe a near degeneracy for the axial-, tensor- and vector-tastes, as predicted by LO rS χ PT [46–48], and the mass splitting between the lightest taste-pseudoscalar and the heaviest taste-singlet pion is $\Delta \approx 300$ MeV. From rS χ PT, sufficiently close to the continuum and chiral limits, the masses-squared of the different pion tastes are given by $(m_\pi^X)^2 = \mu(m_u + m_d) + a^2\Delta_X$ with μ a constant. The mass splitting contribution for each taste, labeled by $X \in (5, \mu 5, \mu\nu, \mu, I)$, reads

$$\Delta_P = 0 \quad (23a)$$

$$\Delta_A = \frac{16}{f^2} (C_1 + 3C_3 + C_4 + 3C_6) \quad (23b)$$

$$\Delta_T = \frac{16}{f^2} (2C_3 + 2C_4 + 4C_6) \quad (23c)$$

$$\Delta_V = \frac{16}{f^2} (C_1 + C_3 + 3C_4 + 3C_6) \quad (23d)$$

$$\Delta_I = \frac{16}{f^2} (4C_3 + 4C_4) , \quad (23e)$$

with f the pion decay constant in the chiral limit and C_i are coefficients defined in Eq. (13) of Ref. [48]. Our data is compatible with this pattern showing that SO(4) taste breaking terms are numerically small. The fact that the mass difference between each multiplet is roughly constant suggests that the coefficient C_4 is numerically dominant. This observation was already made in [46, 48–51] for different discretizations of the action.

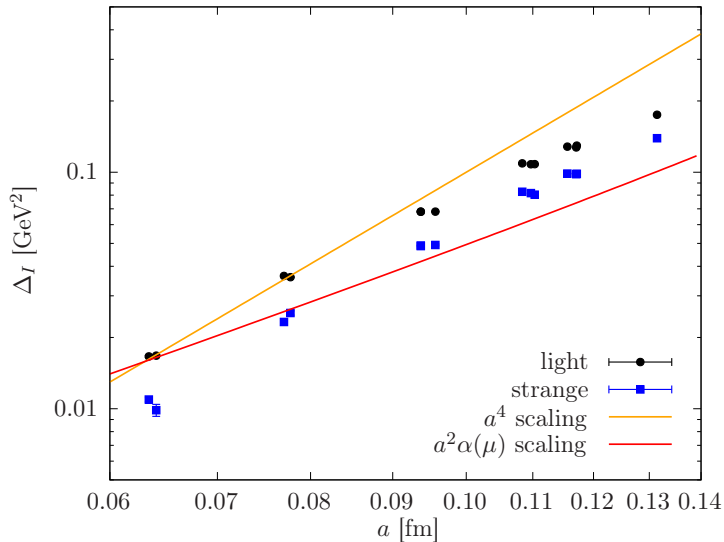


Figure 5. Taste-splitting Δ_I as a function of the lattice spacing. The orange line represents an exact a^4 scaling. Black circles (blue squares) correspond to the light (strange) contribution.

In Fig. 5 we also show the taste-splitting Δ_I as a function of the lattice spacing. At leading order in rS χ PT and in the strong coupling α_s , one expects the mass splitting to scale approximately with $a^2\alpha_s(\mu)$ where α_s is the strong running coupling in the $\overline{\text{MS}}$ scheme evaluated at a scale $\mu \approx 1/a$. As already pointed out in [35], we observe that the taste-splitting decreases much faster than the leading $a^2\alpha_s(\mu)$.

Finally, although the mass splittings Δ_I for mesons composed of two light or two strange quarks are indeed close, we observe a small difference, depicted in Fig. 5. For the taste-singlet η_8 meson, the prediction from rS χ PT is [52]

$$m_{\eta_8,I}^2 = \frac{1}{3}m_{uu,I}^2 + \frac{2}{3}m_{ss,I}^2 \quad (24)$$

and we expect strong taste-breaking effects for the η meson. At our coarsest lattice spacing, $m_{\pi,I} \approx 440$ MeV while the taste-pseudoscalar pion is close to its physical value. Thus we expect discretization effects as large as 140 MeV for the η meson mass at our coarsest lattice spacing.

V. COMPUTATION OF THE MASSES AND AMPLITUDES OF THE η AND η' MESONS

The correlation matrix in Eq. (3) quickly becomes noisy due to the presence of disconnected contributions and it is difficult to find a time interval where the signal is clearly dominated by the ground state while keeping statistical errors under control. In [11, 33], it was observed that excited states mostly contribute to the connected contribution, that can be computed with much higher statistical precision than the disconnected diagrams. We thus remove the excited state contributions in the connected diagrams using the following strategy. At large time, where excited-state contributions are negligible, the connected correlators $\mathcal{C}_l(t)$ and $\mathcal{C}_s(t)$ in Eq. (3) are well-described by a single exponential. In a second step, $\mathcal{C}_l(t)$ and $\mathcal{C}_s(t)$ are replaced by their ground state contribution at times $t > 0$. If the assumption that excited states do not contribute significantly to the disconnected part is correct, we thus expect plateaus at very early times. The validity of this approximation can be tested a posteriori. However, in contrast to the standard effective mass, computed from the unsubtracted correlator, the plateau is not guaranteed to be approached from above.

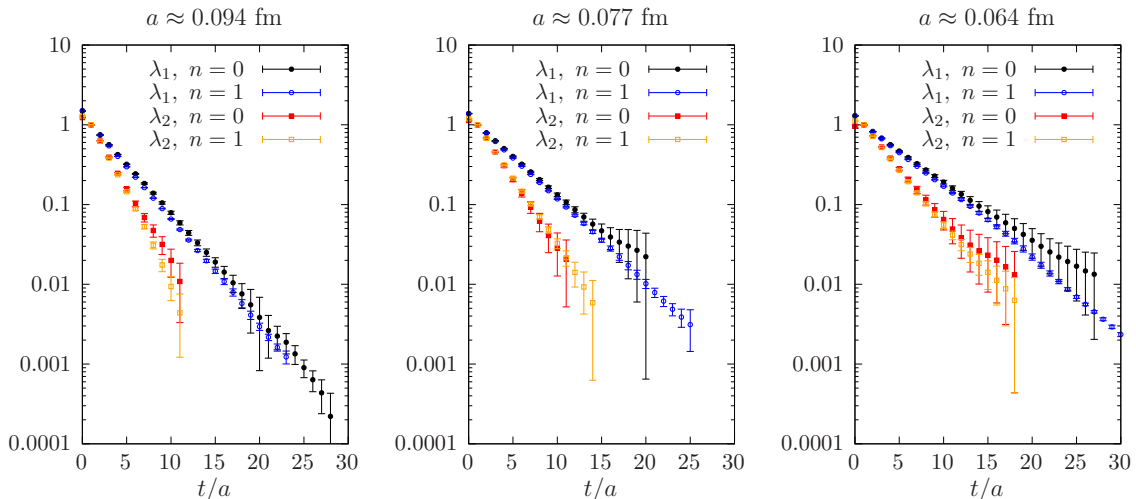


Figure 6. Time dependence of the eigenvalues associated to the η (λ_1) and η' (λ_2) mesons both at vanishing ($n = 0$) and non-vanishing ($n = 1$) momenta where $|\vec{p}| = n(2\pi/L)$. From left to right, our three finest lattice spacings.

A. Extraction of masses and overlaps

In this section, we discuss the two different strategies that have been used to extract the masses and overlap factors of the η and η' mesons.

1. Masses and amplitudes from the GEVP

A well established method to extract information about excited states is to solve the Generalized Eigenvalue Problem (GEVP) [53]

$$C^{2\text{pt}}(t)v_n(t, t_0) = \lambda_n(t, t_0)C^{2\text{pt}}(t_0)v_n(t, t_0), \quad (25)$$

where λ_n and v_n are the eigenvalues and eigenvectors and t_0 is a free parameter. The eigenvectors are normalized such that

$$v_m(t, t_0)^T C^{2\text{pt}}(t_0) v_n(t, t_0) = \delta_{n,m}. \quad (26)$$

In practice, this equation is solved independently for each momentum and the dependence on the momentum is not shown explicitly. In Section II, it was argued that using $C^{2\text{pt}} = \overline{C}$ at vanishing momentum removes possible constant contributions due a partial sampling of the topological charge. In addition, we observe that using $C^{2\text{pt}} = \overline{C}$ leads to smaller statistical error for $\vec{p} = \vec{0}$. Thus, our preferred strategy is to use the combination with $C^{2\text{pt}} = \overline{C}$ at zero momentum and $C^{2\text{pt}} = C$ at non-vanishing momentum. The time dependence of the eigenvalues for a few ensembles is shown in Fig. 6. We observe that the eigenvalues at non-vanishing momentum tend to have smaller statistical uncertainties. During the analysis, we did not see a significant impact on the choice of t_0 . As large values lead to noisy results, we simply set $t_0 = a$ in the following.

The largest eigenvalue is associated with the ground state η meson. A simple estimator of the pseudoscalar meson mass is given by the logarithmic derivative [53]

$$aE_n^{\text{eff}}(t) = \log \frac{\lambda_n(t, t_0)}{\lambda_n(t + a, t_0)}, \quad (27)$$

with $n = \eta, \eta'$. In this equation, the contribution from backward propagating mesons, which is numerically small compared to the statistical error, is neglected. At sufficiently large time, the effective mass can eventually be fitted to a constant. For the η' , we could expect sizable excited states contributions. However, our data suggests a plateau at early times and we are not able

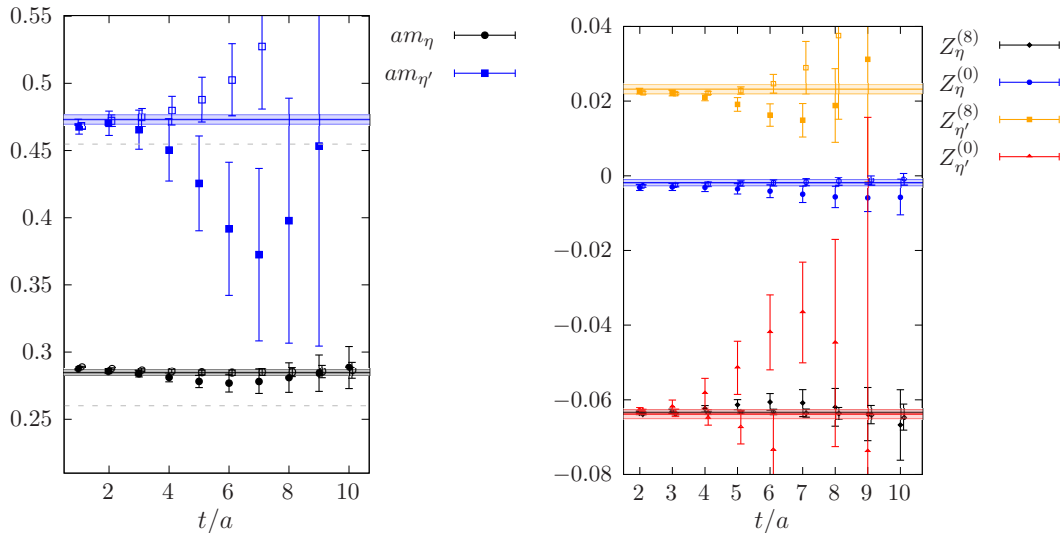


Figure 7. Left: Effective masses at vanishing momentum (filled symbols) and at non-vanishing momentum (open symbols). At non-vanishing momentum, the energies are shifted assuming the continuum relativistic dispersion relation. The bands correspond to our best estimate using a combined fit to both eigenvalues. Right: similar plot for the four overlap factors. The results are given at $a \approx 0.094$ fm.

to resolve these excited states given our statistical precision (see Fig. 7). The overlap factors can be extracted from the eigenvectors through [53]

$$Z_n^{(i)\text{eff}}(t) = \sqrt{2E_n} \left(\frac{\lambda_n(t, t_0)}{\lambda_n(t+a, t_0)} \right)^{(t-t_0/2)/a} \sum_j C_{ij}(t) v_{nj}(t, t_0), \quad (28)$$

where E_n is the energy of eigenstate n extracted using Eq. (27). If the subtracted correlation function \overline{C} is used, the effective overlap factor reads

$$Z_n^{(i)\text{eff}}(t) = \sqrt{2E_n} \left(2 \sinh \left(\frac{E_n \Delta t}{2} \right) \right)^{-1/2} \left(\frac{\lambda_n(t, t_0)}{\lambda_n(t+a, t_0)} \right)^{(t+\Delta t/4-t_0/2)/a} \sum_j \overline{C}_{ij}(t) v_{nj}(t, t_0). \quad (29)$$

and again, plateaus seem to be reached at early times. An appealing feature of this method is the possibility to plot the effective mass or overlap factors as a function of t , making it easier to find a reasonable fit interval. However, these estimators tend to be noisy and the plateaus are lost at early times, especially for the η' meson, as can be seen in Fig. 7.

If one is only interested in the extraction of the meson masses, it is possible to fit the eigenvalues. In that case, we can benefit from having different values of the momenta by performing combined fits and assuming the validity of the continuum dispersion relation. We find that this method leads to better behaved fits. In Fig. 8, we present the results of our correlated fits as a function of t_{\min} , the first time-slice included in the fit and which is chosen to be the same for both momenta. The final value is obtained once a plateau in t_{\min} is observed. The $\chi^2/\text{d.o.f.}$ of all ensembles are in the range [0.6 : 1.9] for the η meson and [0.4 : 1.7] for the η' meson. For comparison, we also present the results obtained by fitting the eigenvalues at a single momentum: within uncertainties, we do not observe any deviation from the continuum dispersion relation and the combined fits tend to be more stables.

2. Fits of the correlation matrix

Instead of solving the GEVP, it is also possible to perform direct fits of the correlation matrix. In this case, we benefit from having two momenta in the extraction of the masses and the overlap

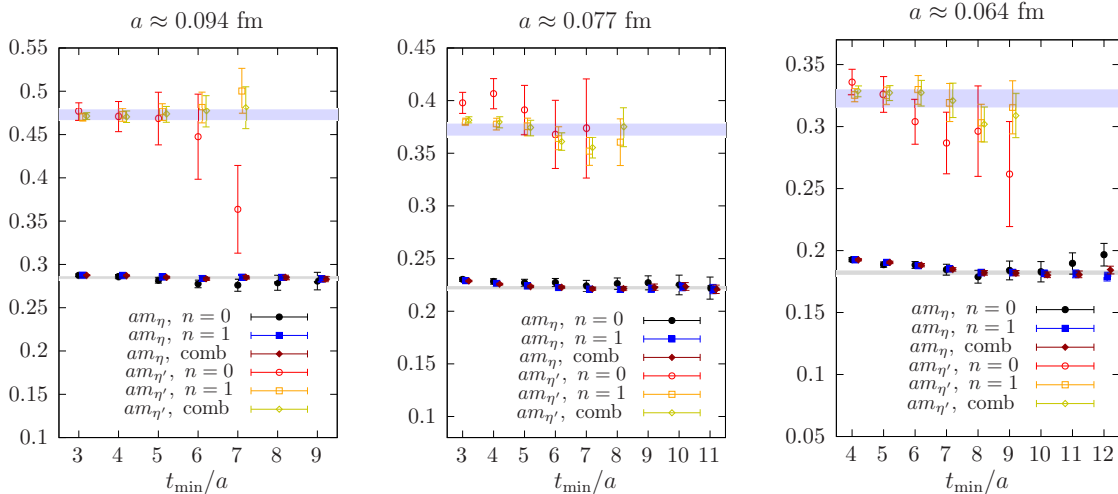


Figure 8. Masses of the η and η' mesons extracted from a fit to the eigenvalues as a function of t_{\min} . For each state we either fit data for $n = 0$, $n = 1$ or both momenta (comb). The bands correspond to our best estimates using the correlator fit method.

factors. Based on Eq. (5), we assume the following fit ansatz, with six independent parameters,

$$C_{ij}(t; \vec{p}) = \frac{Z_{\eta}^{(i)} Z_{\eta}^{(j)}}{2E_{\eta}(\vec{p})} e^{-E_{\eta}(\vec{p})t} + \frac{Z_{\eta'}^{(i)} Z_{\eta'}^{(j)}}{2E_{\eta'}(\vec{p})} e^{-E_{\eta'}(\vec{p})t}, \quad (30)$$

that is expected to provide a good description of our data if higher excited states can be neglected. Assuming the validity of the dispersion relation, it is actually possible to extend the fit to both values of the pseudoscalar momenta without including any new fit parameter. If one considers the subtracted correlation function $\bar{C}(t)$, the fit ansatz becomes

$$\bar{C}_{ij}(t, \vec{p}) = \frac{Z_{\eta}^{(i)} Z_{\eta}^{(j)}}{2E_{\eta}(\vec{p})} \left(1 - e^{-E_{\eta}(\vec{p})\Delta t}\right) e^{-E_{\eta}(\vec{p})t} + \frac{Z_{\eta'}^{(i)} Z_{\eta'}^{(j)}}{2E_{\eta'}(\vec{p})} \left(1 - e^{-E_{\eta'}(\vec{p})\Delta t}\right) e^{-E_{\eta'}(\vec{p})t}. \quad (31)$$

As before, our preferred fit strategy is to use the subtracted correlator \bar{C} at vanishing momentum and the original correlator C at non-vanishing momentum. This is based on the observation that $\bar{C}(t)$ is statistically more precise as compared to $C(t)$ at vanishing momentum. Other combinations have been considered but will only serve as cross-checks in the final continuum extrapolation. Examples of fits are depicted in Fig. 9.

With two momenta, we have to fit six correlators simultaneously. To avoid bias due to by-eye selection and to simplify the fit-range selection, we follow the strategy proposed in [54] and use the Akaike information criterion to select the best fit ranges. In practice, we vary the initial time-slice for each of the six correlators and we associate a weight that depends on the correlated chi-square and the number of degrees of freedom. Explicitly the relative weights are

$$w_i \propto \exp\left(-\frac{1}{2}\text{AIC}\right), \quad \text{AIC} = \chi^2 - n_{\text{data}}, \quad (32)$$

where n_{data} is the total number of point included in the fit. On each ensemble, our final result is obtained by a weighted average over all these fits. In practice we observe that the highest weights have typical chi-squared per degree of freedom in the range $\chi^2/\text{d.o.f.} \in [0.7 : 1.6]$.

In general, we observe that these correlator fits lead to slightly more precise results. A direct comparison of the two different methods analyzed in this work is given in Fig. 10 for our three finest lattice spacings.

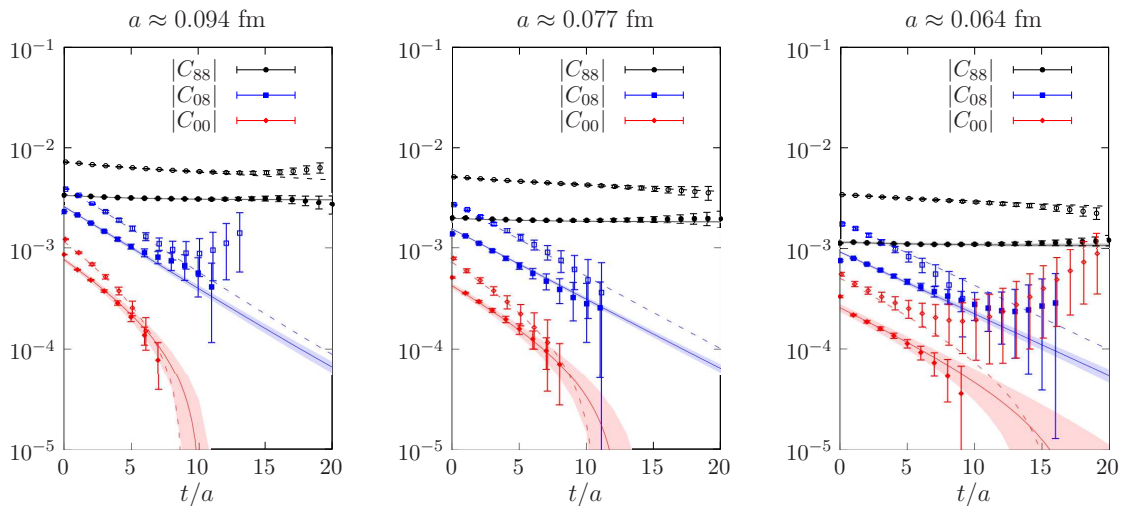


Figure 9. The bands represents the results of a fit to the six correlation functions in Eq. (3) at our three finest lattice spacings as described in the main text. In these fits, $C^{2\text{pt}} = \bar{C}$ and $C^{2\text{pt}} = C$ are used at vanishing (plain symbols) and non-vanishing (open symbols) momenta respectively. For clarity, the correlation functions have been rescaled by a factor $\exp(-\gamma t)$ with some arbitrary γ .

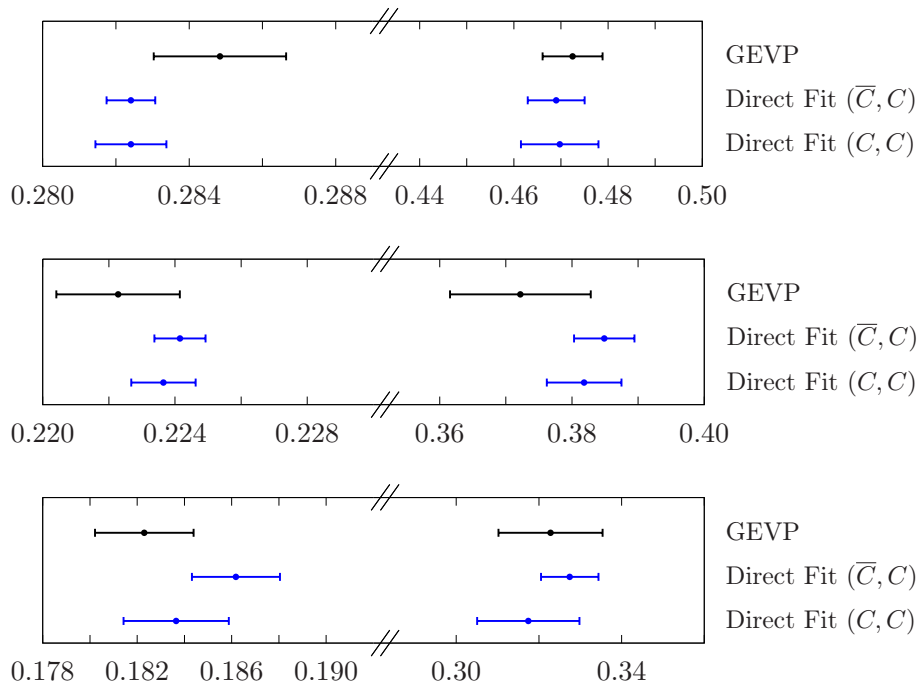


Figure 10. Masses of the η (left) and η' (right) mesons, in lattice units, using the different methods presented in the main text. The black point is obtained from a fit to the eigenvalues. The blue points are obtained from fits of the correlation matrix. The notation (A, B) refers to the correlator (C or \bar{C}) used for $|p| = 0$ and $|p| \neq 0$ respectively. From top to bottom, our three finest lattice spacings.

B. Extrapolation to the continuum limit

To extrapolate our results to the continuum limit, we assume the ansatz

$$m_X(a, X_l, X_s) = m_X^{\text{phys}} + \beta_2(\Lambda a)^2 + \beta_3\alpha_s^n(a^{-1})a^2 + \beta_4(\Lambda a)^4 + \gamma_l X_l + \gamma_s X_s \quad (33)$$

where $n = 2$ or 3 and $\Lambda = 0.5$ GeV is a typical QCD scale. Here, $\alpha_s(a^{-1})$ is the strong coupling constant in the $\overline{\text{MS}}$ scheme evaluated at the scale $1/a$. The quantities X_l and X_s are proxies for

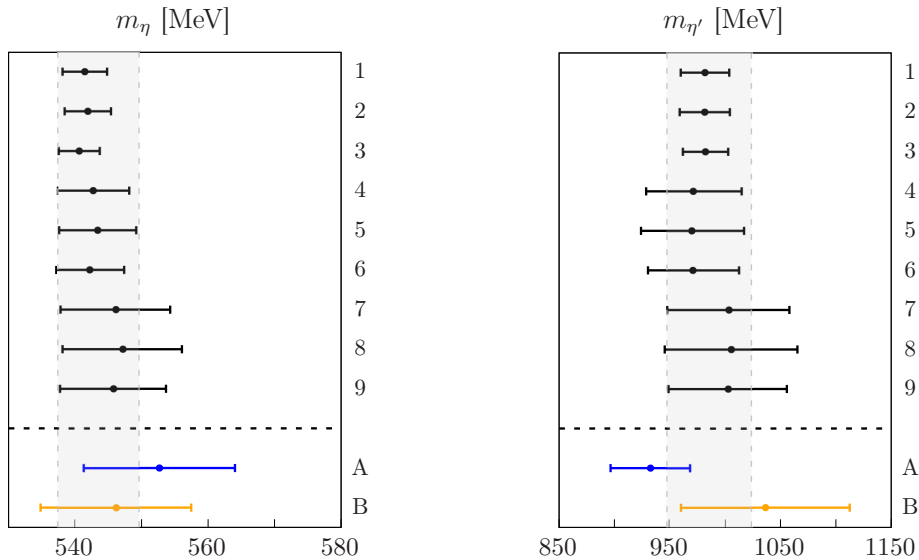


Figure 11. The nine variations used to extrapolate our data to the continuum limit. The labels are explained in the main text. The gray bands represent our total uncertainties. The variation A is the result of our continuum extrapolation when using the GEVP method while the variation B corresponds to the case where the original correlator is used for vanishing momentum.

the slight mistuning of the light and strange quark masses

$$X_l = \frac{M_{\pi_0}^2}{(M_{\pi_0}^{\text{phys}})^2} - 1, \quad X_s = \frac{M_{K_x}^2}{(M_{K_x}^{\text{phys}})^2} - 1 \quad (34)$$

and $M_{K_x}^2 = \frac{1}{2} (M_{K_0}^2 + M_{K_+}^2 - M_{\pi_+}^2)$. See [35] for more details.

In our fits, the correlations between the independent variables a , X_l and X_s are not taken into account. Since the statistical uncertainty associated with the continuum limit is estimated using the jackknife procedure this approximation only prevents us from giving a clear meaning to the quality of the fit. Our set of 13 ensembles, spread among 6 lattice spacings, does not allow to fit β_3 and β_4 simultaneously. We thus estimate the systematic uncertainty by looking at variations keeping either β_3 or β_4 and adding cuts in the lattice spacing. In total, we perform 9 analyses :

- analysis (1) : $\beta_3 = 0$, no cut in the lattice spacing
- analysis (2) : $\beta_4 = 0$, $n = 2$, no cut in the lattice spacing
- analysis (3) : $\beta_4 = 0$, $n = 3$, no cut in the lattice spacing
- analysis (4) : $\beta_3 = 0$, cut at $a = 0.125$ fm
- analysis (5) : $\beta_4 = 0$, $n = 2$, cut at $a = 0.125$ fm
- analysis (6) : $\beta_4 = 0$, $n = 3$, cut at $a = 0.125$ fm
- analysis (7) : $\beta_3 = 0$, cut at $a = 0.113$ fm
- analysis (8) : $\beta_4 = 0$, $n = 2$, cut at $a = 0.113$ fm
- analysis (9) : $\beta_4 = 0$, $n = 3$, cut at $a = 0.113$ fm

and the systematic error is estimated by computing the root-mean-squared deviation of the fit results compared to the flat average. The results obtained for each variation are summarized in Fig. 11. In addition, we show the results of two additional variations called A and B. The result

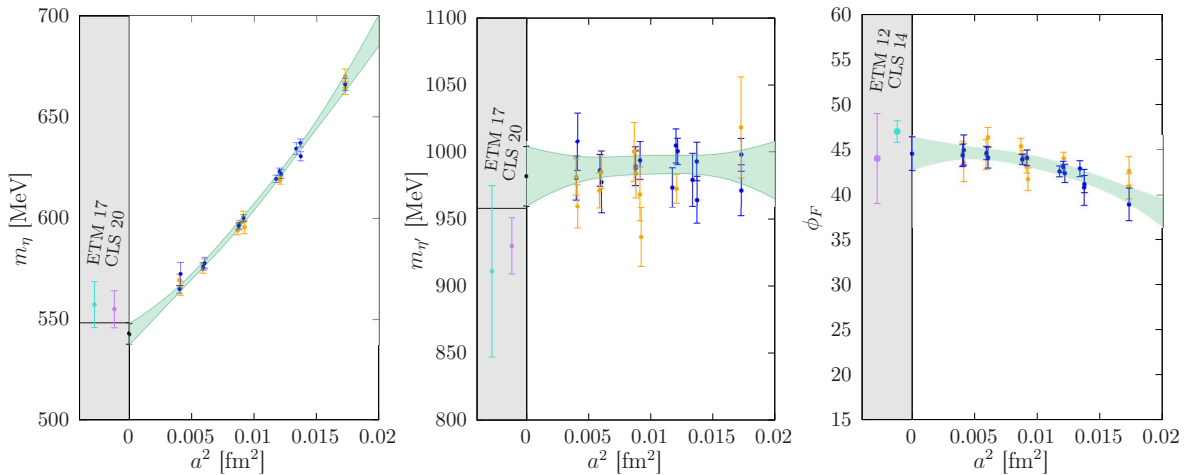


Figure 12. Continuum extrapolation of the η meson mass (left), η' meson mass (middle) and of the mixing angle ϕ_F (right). The blue circles represent the lattice data obtained using large-volume simulation with $L = 6$ fm. The yellow square symbols represents the lattice data obtained using smaller volumes with $L = 3$ fm. Only the large volume ensembles are included in the continuum extrapolation.

A is obtained using the GEVP method described in Section V A 1. The analysis B is the same as the main analysis but using the original correlator C instead of \bar{C} at vanishing momentum. The results agree with the main analysis although with larger statistical errors.

Typical continuum extrapolations, for both the η and the η' , are shown in Fig. 12. For the η meson, we observe a strong dependence on the lattice spacing, as anticipated in Section IV B where we studied the taste-splitting as a function of the lattice spacing. In those fits, we focus on the large volume ensembles with $L \geq 6$ fm and the data-points on smaller physical volumes are only shown for completeness as they are used in our recent work on the pseudoscalar transition form factors [29]. They also indicate that finite-volume effects are small and can be neglected at our level of precision. For the η' pseudoscalar meson, we observe a very mild dependence on the lattice spacing. Again, the results obtained using smaller volumes suggest that finite-volume effects are under control.

Finally, we also present our continuum extrapolation of the mixing angle defined in terms of amplitudes in the flavor basis. The overlap factors play an important role in the extraction of form factors [29].

VI. CONCLUSION

In this paper, we have presented a lattice calculation of the η and η' masses directly at the physical pion mass, using rooted staggered quarks. We have investigated different taste-singlet operators and various noise-reduction methods to compute the quark-disconnected contribution efficiently. The pseudoscalar taste-singlet 4-link operator essentially suppress the staggered oscillations such that the data analysis is greatly simplified. In addition, the VKVR trick [43, 44] can be used to compute the quark-disconnected contribution efficiently. We have computed the masses and the mixing angles (in terms of amplitudes). Those quantities are relevant for the calculation of the pseudoscalar transition form factors that are a key input in the estimate of the pseudoscalar-pole contribution to the hadronic light-by-light scattering in the muon ($g - 2$) [29]. For the η meson, we observe large taste-breaking effects that are due to the use of taste-singlet operators. On the other hand, we observe a very mild continuum extrapolation for the η' meson mass. After extrapolating our data to the continuum limit, we obtain

$$m_\eta = 543.5 \pm 5.2 \pm 2.2_{\text{cont}} [5.6] \text{ MeV}, \quad (35a)$$

$$m_{\eta'} = 986 \pm 35 \pm 14_{\text{cont}} [38] \text{ MeV}, \quad (35b)$$

where the first error is statistical and the second is the systematic uncertainty associated with the continuum extrapolation. The total uncertainty is given in brackets. Those values are compatible with the experimental values $m_\eta = 547.862(17)$ MeV, $m_{\eta'} = 957.78(06)$ MeV [32]. A recent lattice calculation based on $N_f = 2 + 1$ $O(a)$ -improved Wilson-clover ensemble quotes $m_\eta = 554.7(9.2)$ MeV and $m_{\eta'} = 930(21)$ MeV [15]. Using $N_f = 2 + 1 + 1$ twisted-mass fermions, the authors of [12] found $m_\eta = 557(11)$ MeV and $m_{\eta'} = 911(64)$ MeV. Our calculation strongly supports the validity of rooting in the staggered quark formalism. In the future, it would be interesting to extend our study to include decay constants of the singlet mesons [12, 15]. They play an important role in the short distance behavior of the pseudoscalar transition form factors [15, 29], but also in the description of the partial decay widths of pseudoscalar mesons to two photons [29, 55–57].

Regarding the importance of the staggered quarks discretization in precision tests of the Standard Model of particle physics, increasing the precision to provide stronger tests of the rooting procedure is certainly worthwhile. To further improve these results, a larger basis of interpolating operators for the GEVP should enhance the excited state extraction. This could be done using gaussian-smearred correlators or using a combination of the 4-link and 3-link operators that have different couplings to excited states. Also important would be to increase the number of measurements to check for possible long-range autocorrelations, especially in the extraction of the η' meson mass at fine lattice spacings.

ACKNOWLEDGMENTS

We thank all the members of the Budapest-Marseille-Wuppertal collaboration for helpful discussions and the access to the gauge ensembles used in this work. This publication received funding from the Excellence Initiative of Aix-Marseille University - A*Midex, a French “Investissements d’Avenir” programme, AMX-18-ACE-005 and from the French National Research Agency under the contract ANR-20-CE31-0016. The computations were performed on Joliot-Curie at CEA’s TGCC, on Jean Zay at IDRIS, on SuperMUC-NG at Leibniz Supercomputing Centre in München, on HAWK at the High Performance Computing Center in Stuttgart and on JUWELS at Forschungszentrum Jülich. We thank GENCI (grants A0080511504, A0100511504 and A0120511504) and the Gauss Centre for Supercomputing (projects pn73xi and wprecision) for awarding us computer time on these machines. Centre de Calcul Intensif d’Aix-Marseille (CCIAM) is acknowledged for granting access to its high performance computing resources.

-
- [1] S. L. Adler, Axial vector vertex in spinor electrodynamics, *Phys. Rev.* **177**, 2426 (1969).
 - [2] J. S. Bell and R. Jackiw, A PCAC puzzle: $\pi^0 \rightarrow \gamma\gamma$ in the σ model, *Nuovo Cim. A* **60**, 47 (1969).
 - [3] A. A. Belavin, A. M. Polyakov, A. S. Schwartz, and Y. S. Tyupkin, Pseudoparticle Solutions of the Yang-Mills Equations, *Phys. Lett. B* **59**, 85 (1975).
 - [4] G. 't Hooft, Symmetry Breaking Through Bell-Jackiw Anomalies, *Phys. Rev. Lett.* **37**, 8 (1976).
 - [5] F. Chen, X. Jiang, Y. Chen, K.-F. Liu, W. Sun, and Y.-B. Yang, Glueballs at physical pion mass*, *Chin. Phys. C* **47**, 063108 (2023), arXiv:2111.11929 [hep-lat].
 - [6] D. Vadicchino, A review on Glueball hunting, in *39th International Symposium on Lattice Field Theory* (2023) arXiv:2305.04869 [hep-lat].
 - [7] E. Witten, Current Algebra Theorems for the U(1) Goldstone Boson, *Nucl. Phys. B* **156**, 269 (1979).
 - [8] N. H. Christ, C. Dawson, T. Izubuchi, C. Jung, Q. Liu, R. D. Mawhinney, C. T. Sachrajda, A. Soni, and R. Zhou, The η and η' mesons from Lattice QCD, *Phys. Rev. Lett.* **105**, 241601 (2010), arXiv:1002.2999 [hep-lat].
 - [9] H. Fukaya, S. Aoki, G. Cossu, S. Hashimoto, T. Kaneko, and J. Noaki (JLQCD), η' meson mass from topological charge density correlator in QCD, *Phys. Rev. D* **92**, 111501 (2015), arXiv:1509.00944 [hep-lat].
 - [10] K. Ottnad, C. Michael, S. Reker, C. Urbach, C. Michael, S. Reker, and C. Urbach (ETM), η and η' mesons from $N_f = 2 + 1 + 1$ twisted mass lattice QCD, *JHEP* **11**, 048, arXiv:1206.6719 [hep-lat].

- [11] K. Ottnad, C. Urbach, and F. Zimmermann (ETM), A mixed action analysis of η and η' mesons, Nucl. Phys. B **896**, 470 (2015), arXiv:1501.02645 [hep-lat].
- [12] K. Ottnad and C. Urbach (ETM), Flavor-singlet meson decay constants from $N_f = 2 + 1 + 1$ twisted mass lattice QCD, Phys. Rev. D **97**, 054508 (2018), arXiv:1710.07986 [hep-lat].
- [13] J. J. Dudek, R. G. Edwards, P. Guo, and C. E. Thomas (Hadron Spectrum), Toward the excited isoscalar meson spectrum from lattice QCD, Phys. Rev. D **88**, 094505 (2013), arXiv:1309.2608 [hep-lat].
- [14] G. S. Bali, S. Collins, S. Dürr, and I. Kanamori, $D_s \rightarrow \eta, \eta'$ semileptonic decay form factors with disconnected quark loop contributions, Phys. Rev. D **91**, 014503 (2015), arXiv:1406.5449 [hep-lat].
- [15] G. S. Bali, V. Braun, S. Collins, A. Schäfer, and J. Simeth (RQCD), Masses and decay constants of the η and η' mesons from lattice QCD, JHEP **08**, 137, arXiv:2106.05398 [hep-lat].
- [16] E. B. Gregory, A. C. Irving, C. M. Richards, and C. McNeile (UKQCD), A study of the η and η' mesons with improved staggered fermions, Phys. Rev. D **86**, 014504 (2012), arXiv:1112.4384 [hep-lat].
- [17] S. Dürr, Physics of η' with rooted staggered quarks, Phys. Rev. D **85**, 114503 (2012), arXiv:1203.2560 [hep-lat].
- [18] G. C. Donald, C. T. H. Davies, E. Follana, and A. S. Kronfeld, Staggered fermions, zero modes, and flavor-singlet mesons, Phys. Rev. D **84**, 054504 (2011), arXiv:1106.2412 [hep-lat].
- [19] J. B. Kogut and L. Susskind, Hamiltonian Formulation of Wilson's Lattice Gauge Theories, Phys. Rev. D **11**, 395 (1975).
- [20] E. Follana, Q. Mason, C. Davies, K. Hornbostel, G. P. Lepage, J. Shigemitsu, H. Trotter, and K. Wong (HPQCD, UKQCD), Highly improved staggered quarks on the lattice, with applications to charm physics, Phys. Rev. D **75**, 054502 (2007), arXiv:hep-lat/0610092.
- [21] M. Golterman, Staggered fermions, (2024), arXiv:2406.02906 [hep-lat].
- [22] S. R. Sharpe, Rooted staggered fermions: Good, bad or ugly?, PoS **LAT2006**, 022 (2006), arXiv:hep-lat/0610094.
- [23] M. Creutz, Why rooting fails, PoS **LATTICE2007**, 007 (2007), arXiv:0708.1295 [hep-lat].
- [24] M. Creutz, Chiral anomalies and rooted staggered fermions, Phys. Lett. B **649**, 230 (2007), arXiv:hep-lat/0701018.
- [25] C. Bernard, Staggered chiral perturbation theory and the fourth-root trick, Phys. Rev. D **73**, 114503 (2006), arXiv:hep-lat/0603011.
- [26] A. S. Kronfeld, Lattice Gauge Theory with Staggered Fermions: How, Where, and Why (Not), PoS **LATTICE2007**, 016 (2007), arXiv:0711.0699 [hep-lat].
- [27] M. Golterman, QCD with rooted staggered fermions, PoS **CONFINEMENT8**, 014 (2008), arXiv:0812.3110 [hep-ph].
- [28] D. H. Adams, The Rooting issue for a lattice fermion formulation similar to staggered fermions but without taste mixing, Phys. Rev. D **77**, 105024 (2008), arXiv:0802.3029 [hep-lat].
- [29] A. Gérardin, W. E. A. Verplanke, G. Wang, Z. Fodor, J. N. Guenther, L. Lellouch, K. K. Szabo, and L. Varnhorst, Lattice calculation of the π^0 , η and η' transition form factors and the hadronic light-by-light contribution to the muon $g - 2$, (2023), arXiv:2305.04570 [hep-lat].
- [30] A. Gérardin, The anomalous magnetic moment of the muon: status of Lattice QCD calculations, Eur. Phys. J. A **57**, 116 (2021), arXiv:2012.03931 [hep-lat].
- [31] T. Aoyama *et al.*, The anomalous magnetic moment of the muon in the Standard Model, Phys. Rept. **887**, 1 (2020), arXiv:2006.04822 [hep-ph].
- [32] S. Navas *et al.* (Particle Data Group), Review of particle physics, Phys. Rev. D **110**, 030001 (2024).
- [33] C. Michael, K. Ottnad, and C. Urbach (ETM), η and η' mixing from Lattice QCD, Phys. Rev. Lett. **111**, 181602 (2013), arXiv:1310.1207 [hep-lat].
- [34] S. Aoki, H. Fukaya, S. Hashimoto, and T. Onogi, Finite volume QCD at fixed topological charge, Phys. Rev. D **76**, 054508 (2007), arXiv:0707.0396 [hep-lat].
- [35] S. Borsanyi *et al.*, Leading hadronic contribution to the muon magnetic moment from lattice QCD, Nature **593**, 51 (2021), arXiv:2002.12347 [hep-lat].
- [36] S. Borsanyi *et al.* (Budapest-Marseille-Wuppertal), Hadronic vacuum polarization contribution to the anomalous magnetic moments of leptons from first principles, Phys. Rev. Lett. **121**, 022002 (2018), arXiv:1711.04980 [hep-lat].
- [37] R. Altmeyer, K. D. Born, M. Gockeler, R. Horsley, E. Laermann, and G. Schierholz (MT(c)), The Hadron spectrum in QCD with dynamical staggered fermions, Nucl. Phys. B **389**, 445 (1993).
- [38] T. A. DeGrand and S. Schaefer, Improving meson two-point functions by low-mode averaging, Nucl. Phys. B Proc. Suppl. **140**, 296 (2005), arXiv:hep-lat/0409056.
- [39] L. Giusti, P. Hernandez, M. Laine, P. Weisz, and H. Wittig, Low-energy couplings of QCD from current correlators near the chiral limit, JHEP **04**, 013, arXiv:hep-lat/0402002.
- [40] G. S. Bali, S. Collins, and A. Schafer, Effective noise reduction techniques for disconnected loops in

- Lattice QCD, *Comput. Phys. Commun.* **181**, 1570 (2010), arXiv:0910.3970 [hep-lat].
- [41] T. Blum, T. Izubuchi, and E. Shintani, New class of variance-reduction techniques using lattice symmetries, *Phys. Rev. D* **88**, 094503 (2013), arXiv:1208.4349 [hep-lat].
 - [42] E. Shintani, R. Arthur, T. Blum, T. Izubuchi, C. Jung, and C. Lehner, Covariant approximation averaging, *Phys. Rev. D* **91**, 114511 (2015), arXiv:1402.0244 [hep-lat].
 - [43] L. Venkataraman and G. Kilcup, The eta-prime meson with staggered fermions, (1997), arXiv:hep-lat/9711006.
 - [44] E. B. Gregory, A. C. Irving, C. M. Richards, and C. McNeile, Methods for Pseudoscalar Flavour-Singlet Mesons with Staggered Fermions, *Phys. Rev. D* **77**, 065019 (2008), arXiv:0709.4224 [hep-lat].
 - [45] L. Giusti, T. Harris, A. Nada, and S. Schaefer, Frequency-splitting estimators of single-propagator traces, *Eur. Phys. J. C* **79**, 586 (2019), arXiv:1903.10447 [hep-lat].
 - [46] W.-J. Lee and S. R. Sharpe, Partial flavor symmetry restoration for chiral staggered fermions, *Phys. Rev. D* **60**, 114503 (1999), arXiv:hep-lat/9905023.
 - [47] C. Bernard (MILC), Chiral logs in the presence of staggered flavor symmetry breaking, *Phys. Rev. D* **65**, 054031 (2002), arXiv:hep-lat/0111051.
 - [48] C. Aubin and C. Bernard, Pion and kaon masses in staggered chiral perturbation theory, *Phys. Rev. D* **68**, 034014 (2003), arXiv:hep-lat/0304014.
 - [49] C. W. Bernard, T. Burch, K. Orginos, D. Toussaint, T. A. DeGrand, C. E. Detar, S. Datta, S. A. Gottlieb, U. M. Heller, and R. Sugar, The QCD spectrum with three quark flavors, *Phys. Rev. D* **64**, 054506 (2001), arXiv:hep-lat/0104002.
 - [50] C. Aubin, C. Bernard, C. DeTar, J. Osborn, S. Gottlieb, E. B. Gregory, D. Toussaint, U. M. Heller, J. E. Hetrick, and R. Sugar, Light hadrons with improved staggered quarks: Approaching the continuum limit, *Phys. Rev. D* **70**, 094505 (2004), arXiv:hep-lat/0402030.
 - [51] C. Aubin, T. Blum, M. Golterman, and S. Peris, Muon anomalous magnetic moment with staggered fermions: Is the lattice spacing small enough?, *Phys. Rev. D* **106**, 054503 (2022), arXiv:2204.12256 [hep-lat].
 - [52] C. Bernard, C. E. DeTar, Z. Fu, and S. Prelovsek, Scalar meson spectroscopy with lattice staggered fermions, *Phys. Rev. D* **76**, 094504 (2007), arXiv:0707.2402 [hep-lat].
 - [53] B. Blossier, M. Della Morte, G. von Hippel, T. Mendes, and R. Sommer, On the generalized eigenvalue method for energies and matrix elements in lattice field theory, *JHEP* **04**, 094, arXiv:0902.1265 [hep-lat].
 - [54] W. I. Jay and E. T. Neil, Bayesian model averaging for analysis of lattice field theory results, *Phys. Rev. D* **103**, 114502 (2021), arXiv:2008.01069 [stat.ME].
 - [55] A. Gérardin, H. B. Meyer, and A. Nyffeler, Lattice calculation of the pion transition form factor with $N_f = 2 + 1$ Wilson quarks, *Phys. Rev. D* **100**, 034520 (2019), arXiv:1903.09471 [hep-lat].
 - [56] C. Alexandrou *et al.* (Extended Twisted Mass), $\eta \rightarrow \gamma^* \gamma^*$ transition form factor and the hadronic light-by-light η -pole contribution to the muon $g-2$ from lattice QCD, *Phys. Rev. D* **108**, 054509 (2023).
 - [57] C. Alexandrou *et al.*, Pion Transition Form Factor from Twisted-Mass Lattice QCD and the Hadronic Light-by-Light π^0 -pole Contribution to the Muon $g - 2$, (2023), arXiv:2308.12458 [hep-lat].